# A New Multi-Scale Model Based on CFD and Macroscopic Calculation for Corrugated Structured Packing Column

**B. Sun**
State Key Laboratory of Chemical Engineering, School of Chemical Engineering and Technology, Tianjin University, Tianjin 300072, China

**L. He**
Peiyang Chemical Equipment Co., Ltd, Tianjin 300072, China

**B.T. Liu**
State Key Laboratory of Chemical Engineering, School of Chemical Engineering and Technology, Tianjin University, Tianjin 300072, China

**F. Gu**
Tianjin Internal Combustion Engine Research Institute, Tianjin 300072, China

**C.J. Liu**
State Key Laboratory of Chemical Engineering, School of Chemical Engineering and Technology, Tianjin University, Tianjin 300072, China

*DOI 10.1002/aic.14082*
*Published online March 16, 2013 in Wiley Online Library (wileyonlinelibrary.com)*

*A multi-scale approach with the combination of computational fluid dynamic (CFD) and macroscopic calculation methods has been proposed to predict the hydrodynamics behavior in the corrugated structured packing column. On the basis of the concept of the representative unit, the three-dimensional (3-D) volume of fluid (VOF) model of the structured packing is applied in the small scale simulation, and the stream split fraction coefficients and effective wetted area ratio are calculated. The unit network model, which is a mechanistic model, is applied in large scale calculation basing on the small scale results. The liquid holdup distribution in the entire column can be available by this multi-scale method. A comparison between the simulation results and the experimental data of our previous work is given to validate the present model. The multi-scale model is proved to be prospective to assist the analysis and design of structure packing columns in chemical engineering.* © 2013 American Institute of Chemical Engineers *AIChE J*, 59: 3119–3130, 2013
*Keywords: multi-scale model, CFD, macroscopic calculation, stream split fraction coefficients, structured packing*

## Introduction

Structured packing column is commonly used in unit operations such as distillation and absorption etc., and the structured packing column has the advantages of large capacity, low pressure drop, and high efficiency.[1] It is found that the maldistribution of liquid and vapor phase on structured packings is the cause of the poor performance of the industrial scale column. Detailed investigations of the fluid dynamic behavior and mass-transfer behavior in structured packing columns have been focused by many authors for predicting the process performance or dealing with the scale-up problem. Some empirical models, such as Billet[2], SRP[3,4], and Delft[5] models were proposed to predict the performance in the packed column basing on the experimental data, but their successful applications are still limited within certain working conditions.

In the past decades, with the development of computer techniques, computational fluid dynamic (CFD) method has become a powerful implement applied by more and more researchers to simulate the fluid flow in the structured packing columns. Hodson et al.[6] maybe the first authors who introduced the CFD method to investigate the performance of the structured packing column and the flow pattern of vapor phase within the channel simulated by Phoenics code. For simulating the hydrodynamics of liquid phase flow in structured packing filled with catalyst pellets, van Gulijk[7] put forward a Toblerone model, simplified the multi-phase flow to a single phase in the channels, and calculated the transversal dispersion in the structured packed bed using the CFX code. On the basis of van Gulijk's research, the group of Krishna[8–10] carried out a number of experimental and theoretical studies to investigate the flow and mass-transfer behavior within a KATAPAK-S structure packed with catalyst. Klöker and coworkers[11–13] proposed an innovative approach for the design of reactive distillation column internals and CFD simulations, which was regarded as a virtual experiment for providing the necessary hydrodynamic and mass-transfer correlations. Petre and coworkers[14,15] abstracted five types of

Correspondence concerning this article should be addressed to B.T. Liu at liubotan@tju.edu.cn.

representative units (REU) from a large amount of repetitive packing structures, and calculated the pressure drop of the REUs using CFD code FLUENT. Then the total bed pressure drop could also be calculated according to the pressure loss coefficient in each particular REU. Raynal et al.[16] made research in the influence of mesh size and turbulence models on the dry pressure drop of structured packing, and they considered $k$–$\varepsilon$ RNG model as the most appropriate model in the simulation of the column pressure drop. Khosravi et al.[17] compared the results of different turbulent models by CFX, and they are inclined to believe $k$–$\omega$ model as the best one. In their work, a whole packing module is modeled and the total grid number is as much as 7,000,000 to determine the pressure drop. While for mass- and heat-transfer processes, a mesh of 1,000,000 cells was adopted. This may denote the high computing costs which need to overcome when structured packing using CFD is studied. Similar problems also exist in other researchers' work. Fernandes et al.[18,19] studied the structured packing column for supercritical extraction using CFD method, and the whole module of structured packing model included 2,000,000 tetrahedral cells. So as it can be seen, the problem of high computing cost may be the barrier of application of CFD method on the industrial scale column.

For simulating the two-phase flow within a structured packing bed, the volume of fluid (VOF) approach is mostly chosen to track the gas–liquid interface. Szulczewska et al.[20] and Gu et al.[21] built a two-dimensional (2-D) model to find out the interfacial area and the mechanism of falling film on the corrugated plate. Raynal et al.[22] believed that the flow path of gas–liquid flow within the structured packing bed can be simplified into a 2-D zigzag channel, and the VOF approach was implemented in their investigation to estimate the thickness of falling film and the liquid holdup. Valluri et al.[23] and Haroun et al.[24] simulated the liquid film flow behavior on the surface of structured packing sheet and found recirculation zone at the wave trough at certain $Re$ numbers. Chen et al.[25,26] modeled the exact packing surface geometry and simulated the gas–liquid flow and mass transfer on the structured packing sheet three dimensionally with VOF approach. In summary, VOF approach is able to reveal the flowing details, and it can supply useful information such as flow patterns, wetting area, etc. However, this method requires the geometry of the packing element cells be exactly modeled, and thus the simulation should be confined to a small volume.

Accordingly, the published work reveal the simulation of structured packing using CFD method can only reflect the information in a very small sections of the packing by far, which constraints to the computing power. As Mahr and Mewes[27] pointed out, for columns of technical dimensions with today's computing power, modeling two-phase flow at the scale of the exact packing geometry has not been feasible yet, while in practical applications, the parameters of the whole column, such as pressure drop, separation performance, and backing mixing are always focused, especially in the process of designing. For this aspect, it is recognized that another type of macro-scale models, namely, the mechanistic models[28] are feasible for the whole column simulation with much less computing cost. However, these types of models depend on the experimental data to regress the model parameters, which also limits their applications.

The current problem is how to simulate the structured packing column at large scale with the account for the phenomena inside very particular elements under a computing power available for a common researcher. Very naturally, it comes to multi-scale approaches. Raynal and Royon-Lebraud[29] have proposed a multi-scale approach which is solely based on the CFD method. In their study, the 2-D VOF approach was applied for small scale for two-phase flow within packing element. The result of the VOF calculation was put into use for pressure drop prediction of one packing layer by pseudo single phase CFD simulation. The result of the second step is summarized to a resistance coefficient and employed in large scale CFD simulation to predict the whole column pressure drop. As for the last step, the exact geometry of packing was not necessary to be modeled. In the present study, a multi-scale approach is proposed, and the small scale simulation is 3-D VOF simulation of the two-phase flow within the element cells with the exact geometry modeled. A mechanistic model is adopted in large scale calculation, and the parameters of the mechanistic model come from the result of the small scale simulation of the research. A comparison between the simulation results and the experimental data of our previous work is given to validate the present model.

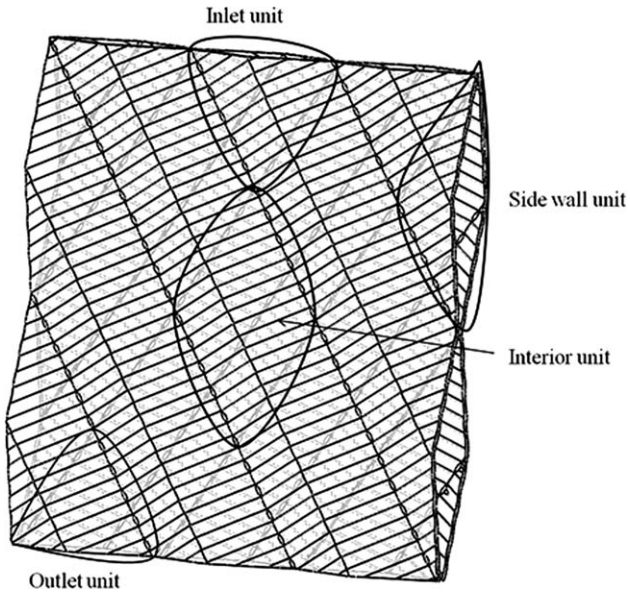

**Figure 1. Four kinds of representative units.**

## Multi-scale Calculation Strategy

### *Representative unit*

The concept of the representative unit is not a new one. Early in 2003, Petre et al.[14,15] submitted this concept in their study, which is analogous to the intersections or nodes of the mechanistic models. It is not complicated to find that the structured packing is composed by lots of repeated structures with similar boundary conditions. In this study, four types of representative units are concluded, and they are respectively named as inlet, outlet, side wall, and interior unit. The structures of the representative units are shown in Figure 1. These four types of units correspond to the position of inlet, outlet, side wall, and interior of the packing simultaneously. The interior unit refers to the element space formed by two pieces of structured packing sheet, and the contact point of two pieces of packing sheets is defined as node.

For any unit, the inlet condition is determined by the outlet flow behavior in the upper unit, and the outlet condition of a unit is also the feeding condition of the lower one. The liquid distribution in an interior unit is affected by three

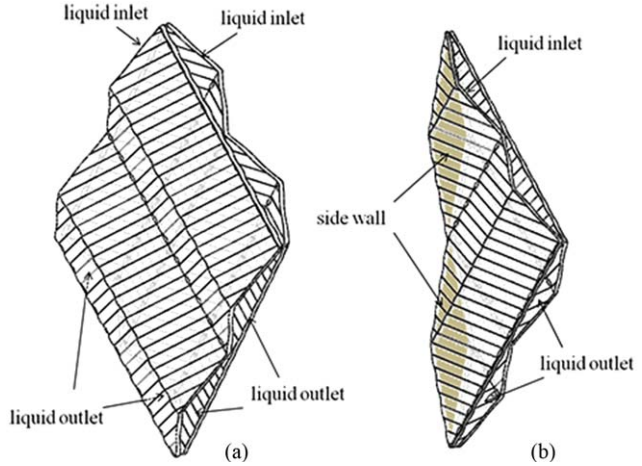


**Figure 2. Physical models.**

**(a) Interior unit model, (b) Side wall unit model.**

upper interior units, but for side wall unit, only a side wall unit and an interior unit exert the influence on it. For the inlet unit, feed is assumed to be uniform and evenly distributed in two different channels. While for the outlet unit, there is no need to know the outlet liquid distribution performance as a result of no lower unit. Based on the above perspectives, only two physical models need to be taken into account to investigate the liquid distribution behavior, that is, one is interior unit model, and the other is side wall unit model as shown in Figure 2.

It must be noted that the unit models for CFD computing in this work contains a few cells, which is different from Petre's[14,15] concept.

The packing applied in this article is Mellapak 350X corrugated sheet structured packing, and the structure parameters are list in Table 1.

Figure 3 gives the calculation strategy of the multi-scale method. A 3-D CFD model which depicts the gas–liquid two-phase flow in small scale is proposed for the first time, and it is calculated to obtain the stream split fraction coefficients. Then, with a newly defined liquid distribution model and the coefficients obtained in small-scaled simulation, a macro-scale calculation is conducted to display the liquid distribution and holdup in the entire column. The result of the multi-scaled calculation is of great value to the optimum design of the column in chemical engineering.

### *Small scale calculation: CFD model*

To make the simulation sufficiently fundamental, i.e., take enough consideration to the effect of geometry on the liquid and vapor distribution, the VOF method is chosen to depict the gas–liquid two-phase flow inside the representative units. The commercial CFD code FLUENT is applied and RNG $k$–$\varepsilon$ turbulence model is adopted to describe the turbulent flow on the packing. The basic model equations are written as follows.

The volume fraction equation is

$$\frac{1}{\rho_{\mathrm{q}}}\left[\frac{\partial}{\partial t}\left(\alpha_q\rho_q\right)+\nabla\cdot\left(\alpha_q\rho_q\vec{v}_q\right)=S_{\alpha_q}+\sum_{p=1}^{n}\left(\dot{m}_{pq}-\dot{m}_{qp}\right)\right] \quad (1)$$

where $q$ = L, G.

The momentum transport equation is

$$\frac{\partial}{\partial t}(\rho\vec{u})+\nabla\cdot(\rho\vec{u}\vec{u})=-\nabla P+\nabla\cdot\left[\mu\left(\nabla\vec{u}+\vec{u}^{T}\right)\right]+\rho\vec{g}+\vec{F} \quad (2)$$

The momentum equation depends on the phase volume fraction because the physical properties in the momentum equation are calculated as volume-fraction-weighted averages over each phase. The average density $\rho$ and viscosity $\mu$ are given by Eqs. 3 and 4

$$\rho=\alpha_{\mathrm{L}}\rho_{\mathrm{L}}+(1-\alpha_{\mathrm{L}})\rho_{\mathrm{G}} \quad (3)$$

$$\mu=\alpha_{\mathrm{L}}\mu_{\mathrm{L}}+(1-\alpha_{\mathrm{G}})\mu_{\mathrm{G}} \quad (4)$$

The source term $F$ of the momentum equation in our research only arises from the surface tension ($F_{\mathrm{VOL}}$) and drag force ($F_{\mathrm{LG}}$).

For thin film flow, the effect of surface tension can be significant.[30] FLUENT includes the effects of surface tension as a body force in the momentum equation according to the method proposed by Brackbill et al.[31]. This technique interprets surface tension forces as a continuous volume forces, and it is defined as

$$F_{\mathrm{VOL}}=\sigma_{\mathrm{ij}}\frac{\rho\kappa_i\nabla\alpha_i}{0.5\left(\rho_i+\rho_j\right)} \quad (5)$$

where $\sigma$ is the surface tension coefficient, and $\kappa$ is the free surface curvature, which is defined as

$$\kappa=\nabla\cdot\hat{n}=\frac{1}{|n|}\left[\left(\frac{n}{|n|}\cdot\nabla\right)|n|-(\nabla\cdot n)\right] \quad (6)$$

where $\hat{n}$ is the divergence of the unit normal, and $\hat{n}=n/|n|$, $n=\nabla\alpha_q$.

The unit surface normal at the live cell next to the wall is replaced by the following equation

$$\hat{n}=\hat{n}_{\mathrm{w}}\cos\theta+\hat{t}_{\mathrm{w}}\sin\theta \quad (7)$$

where $\hat{n}_{\mathrm{w}}$and $\hat{t}_{\mathrm{w}}$are the unit vectors normal to and tangential to the wall, respectively. The contact angle $\theta$ is the angle between the wall and the tangent to the interface at the wall.

The influence of the drag force can be described by the friction pressure drop model developed by Woerlee[32], and then it can be depicted in Eq. 8

$$F_{\mathrm{LG}}=-\alpha_{\mathrm{e}}f_{\mathrm{i}}\rho_{\mathrm{G}}(u_{\mathrm{G}}-u_{\mathrm{L}})|u_{\mathrm{G}}-u_{\mathrm{L}}| \quad (8)$$

where $a_{\mathrm{e}}$ is the effective interfacial area per unit volume and it can be calculated by $\alpha_{\mathrm{e}}=|\nabla\alpha_{\mathrm{G}}|=|\nabla\alpha_{\mathrm{L}}|$[33]. $f_{\mathrm{i}}$ is the interfacial friction factor. Stephan and Mayinger[34] developed a new correlation to give a description of the interfacial friction in countercurrent flow which can be shown as follows

$$f_{\mathrm{i}}=0.079Re_{\mathrm{G}}^{-0.25}\left(1+115\delta^{*N}\right) \quad (9)$$

where$Re_{\mathrm{G}}=u_{\mathrm{G}}\rho_{\mathrm{G}}(D-2\delta)/\mu_{\mathrm{G}}$ and $N=3.95(1.8+3/D^{*})$. $D^{*}$ and $\delta^{*}$ are the dimensionless ratios of tube diameter and film

**Table 1. Structure Parameters of Mellapak 350X**

| Crimp height, $h$ (mm) | Channel base, $B$ (mm) | Channel side, $S$ (mm) | Specific area, $a_{\mathrm{p}}$ ($\mathrm{m^2/m^3}$) | Porosity, $\varepsilon$ (%) | Corrugation angle, $\theta$ (°) |
|---|---|---|---|---|---|
| 8.7 | 18.8 | 12.8 | 350 | 94 | 60 |

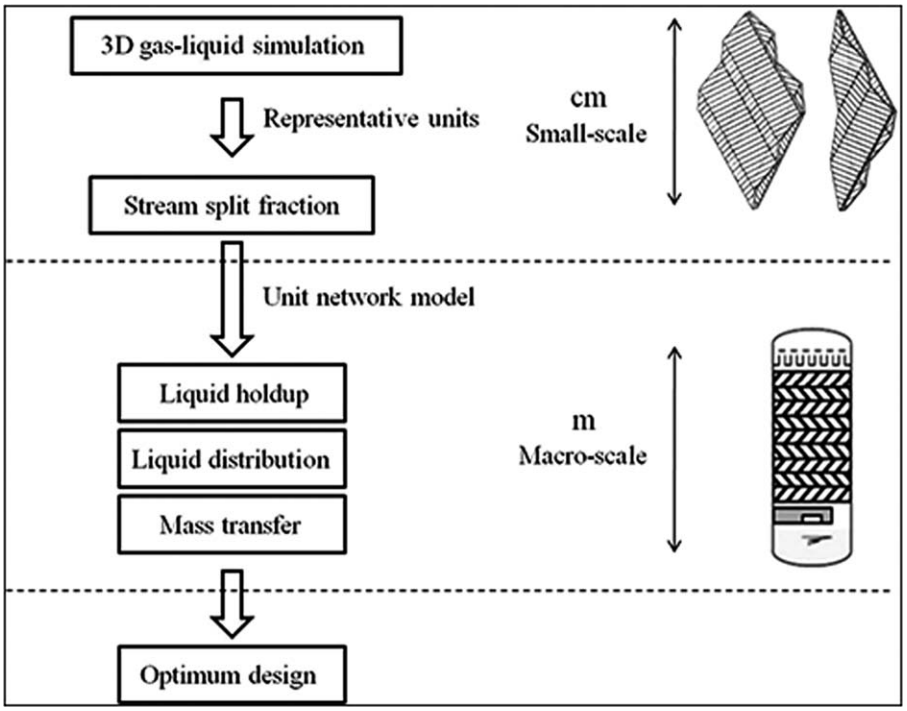


**Figure 3. The strategy chart of the multi-scale method.**

thickness to the Laplace length $[\sigma/(\rho_L-\rho_G)g]^{0.5}$, respectively. The tube diameter $D$ is replaced by the hydrodynamic diameter $d$ of the packing unit, and its value can be considered as the channel side of the packing unit ($S$). $\delta$ is calculated by Nusselt film thickness[35], and it is defined as $\delta=\left[3\mu q/(\rho_G g\cos\theta)\right]^{0.333}$. Where $q$ is the volume flow rate per unit of perimeter length, $\theta$ is the corrugation angle of packing.

The turbulent kinetic energy ($k$) equation and turbulent dissipation rate ($k$) equation are

$$\rho\frac{dk}{dt}=\frac{\partial}{\partial x_i}\left[\alpha_k\mu_{\text{eff}}\frac{\partial k}{\partial x_i}\right]+G_k-\rho\varepsilon \tag{10}$$

$$\rho\frac{d\varepsilon}{dt}=\frac{\partial}{\partial x_i}\left[\alpha_\varepsilon\mu_{\text{eff}}\frac{\partial \varepsilon}{\partial x_i}\right]+C_{1\varepsilon}\frac{\varepsilon}{k}G_k-C_{2\varepsilon}\rho\frac{\varepsilon^2}{k}-R \tag{11}$$

where $\alpha$ is the reciprocal of effective Prandtl number. $G_k$ is the turbulence kinetic energy caused by averaged velocity gradient. $C_{1\varepsilon}$ and $C_{2\varepsilon}$ are constant as 1.44 and 1.92, respectively.

The unstructured grid generation technique is applied to deal with the complex geometrical structure. The grid numbers of the models shown in Figure 2a and b are 100,000 and 68,000, respectively.

In the simulation, the geo-reconstruct method is employed to trace the gas–liquid interface precisely, and the time step size is set as $1\times10^{-5}$ s. First-order upwind differencing is chosen as the solution of momentum equation. The Body Force Weighted method is implemented for pressure discretization, and Pressure Implicit with Splitting of Operators method is adopted for pressure–velocity coupling.

Water–air system is selected, and the fluid properties ($\rho$, $\mu$, $\sigma$) are set to be constant, which are equal to the fluid properties at 20°C. The liquid–solid contact angle is 57°. For model shown in Figure 2a, there are two liquid inlets which cling to the two channels in the top interior unit. For the model shown in Figure 2b, only one liquid inlet exists in the top side wall unit. The width of the liquid inlet is 1 mm. In the present study, a wide range of liquid spray density from 10 to 100 $m^3/(m^2\ h)$ is applied, which is conducted to investigate the stream split fraction coefficients, and it is extended from 10 to 150 $m^3/(m^2\ h)$ to obtain the data of the effective wetting area ratio. The large liquid spray density corresponds to the industrial background of absorption processes, in which the liquid load can be very large, especially for the $CO_2$ capture process, the liquid spray density varies from 10 to 250 $m^3/(m^2\ h)$[24,29]. Another reason is that the liquid load applied in Gu's[36] experiment, which is used to validate the present model, varies from 30 to 100 $m^3/(m^2\ h)$.

### *Macro-scale calculation: unit network model*

The macro-scale calculation is based on a newly established mechanistic model: unit network model. In this model, each element cell in the structured packing can be defined by indicators $i$, $j$, and $k$, and the directions are indicated in Figure 4.

The unit network model is based on the following assumptions:

1. Once the liquid flows into the packing unit, the mixing and distribution of the liquid happens only in the unit, and it is not influenced by other units around.
2. The liquid distribution in a unit can be divided into three parts, namely, flowing along the channel, transverse flow, and flowing downwards across the node.
3. The liquid flowing downward across the node is evenly split into two parts, and then flowing along the two channels in the lower unit.
4. Liquid at the column side is partly reflected to the center of the column.

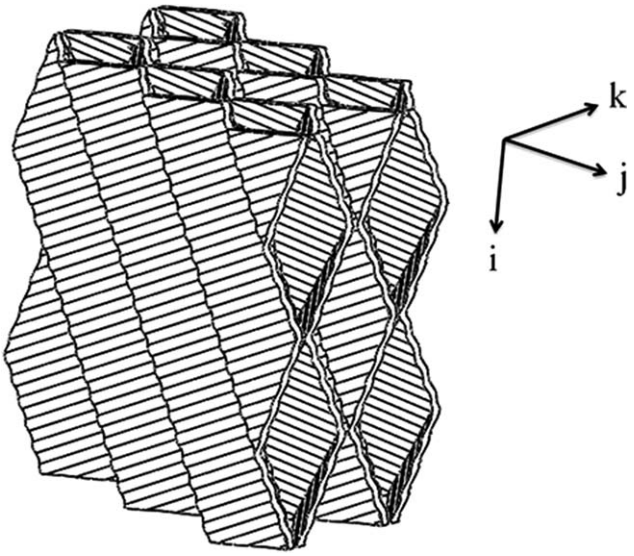


**Figure 4. Direction of the packing calculated.**

The assumption 2 suggests all the possible stream split manners corresponding to the packing surface without holes. Obviously, it is flexible in other cases. Based on the assumption 2, three stream split fraction coefficients $f$, $h$, and $g$ are introduced to describe the proportion of liquid flowing along the channel, the transverse flow, and the liquid flowing downwards across the node, respectively. The relationship is $f + h + g = 1$. While for the side wall unit, the case is totally different. First, the proportion of transverse flow is different and another parameter $hr$ is defined to distinguish with that in interior unit; second, the liquid flowing downwards splits up in a different manner with that in interior unit. As for the interior unit, the liquid downwards across the node is actually divided into two streams along two sheets, respectively, in the unit below. In this work, these two streams are assumed to be equal in flow rate, as depicted in assumption 3; but for the side wall unit, the liquid flow downwards flows across the node and then splits up into one stream on the column wall, and another stream reflected back to column interior along the adjacent sheet, as depicted in assumption 4. A parameter $r$ is defined to represent the reflected part of the liquid flow.

The liquid distribution can be determined with the assumptions above. The liquid distribution law in the interior unit as well as side wall unit is illustrated in Figure 5. A–D represents the cells included in interior or side wall units. In this article, $L$ and $R$ are defined as the liquid flowing along the left-inclining and right-inclining channels, respectively. $G$ is defined as the liquid flowing vertical downward. For the side wall unit, $LWL$ and $LWR$ represent the liquid flowing close to the left and right column wall.

The details of how the liquid in the original cell (A) flows into the neighboring lower cells B, C, or D is revealed in Figure 5. Figure 5a shows that, in side wall unit, there are two streams on the opposite sheets flowing out the original cell (A). One stream flows down along the left wall, and is defined as ($LWL$_A (1)). Here (1) is the stream number, and $LWL$_A is the quantity. The rest of this section can be deduced in the same manner, thus it is not explained or discussed again in the article. The other stream flows along the right-inclining channel, and it is defined as ($R$_A (2)). Then ($LWL$_A (1)) is divided into two parts: one stream (3) flows downward to D and the quantity is $LWL$_A*$(1 - hr)$, and it is defined as ($LWL$_A*$(1 - hr)$ (3)); the other stream ($LWL$_A*$hr$ (4)) firstly flows transverse to C, and then flows along the left-inclining channel to D. The two streams converge into one, and then they are reassigned to two streams at the node again. One stream ($LWL$_A*(1-$r$) (8)) flow continuously down along the left wall, and the other one ($LWL$_A*$r$ (9)) is reflected to the column along the right-inclining channel of D. ($R$_A (2)) is divided into three streams in C. The first stream ($R$_A*$f$ (7)) flows continuously along the right-inclining channel of C, the second stream ($R$_A*$g$ (6)) flows downward to the node at the bottom of C, the third stream ($R$_A*$h$ (5)) flows transverse to D and flows along the right-inclining channel of D. For the interior unit revealed in Figure 5b, the two streams in the original cell (A) are along the two channels, and the developing of these two streams is similar to that of $R$_A (2) in side wall unit.

## Simulation Results

### *Hydrodynamic behavior analysis*

The liquid film flow behavior in different spray density and unit models is depicted in Figures 6a–d. In side wall model, especially for the water–air system, most liquid flows along the side wall, and it is reflected to the right-inclining channel of the lower side wall unit. No liquid can be observed to flow transverse. In Figures 6c, d, most liquid flows along the channel down to the lower unit, only a small fraction of it flows transverse and vertical downwards. The flow pattern of the liquid flowing downward and transverse is changed from the film flow to mist flow as a result of the small flow rate. In addition, the increased flow rate of liquid has little effect on the distribution result.

### *Stream split fraction coefficients*

The result of the stream split fraction coefficients in different spray densities ($L$) are shown in Figure 7. As mentioned above, most liquid flows along the channel, and this leads to a higher value of $f$. The value of $h$ and $hr$ are less

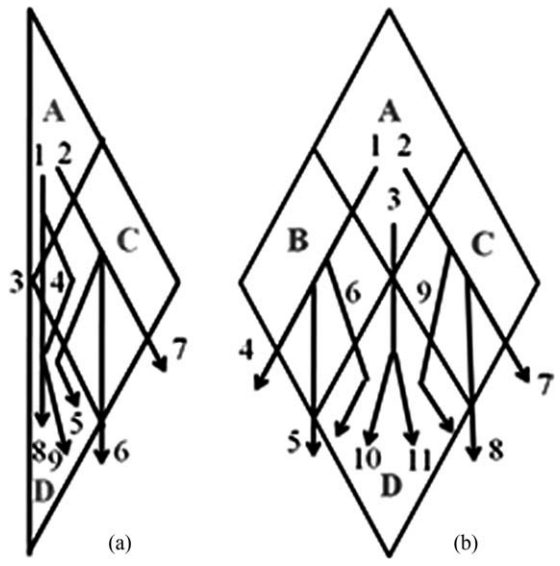


**Figure 5. Liquid distribution law of the unit network model.**

**(a) Side wall unit model, (b) Interior unit model**

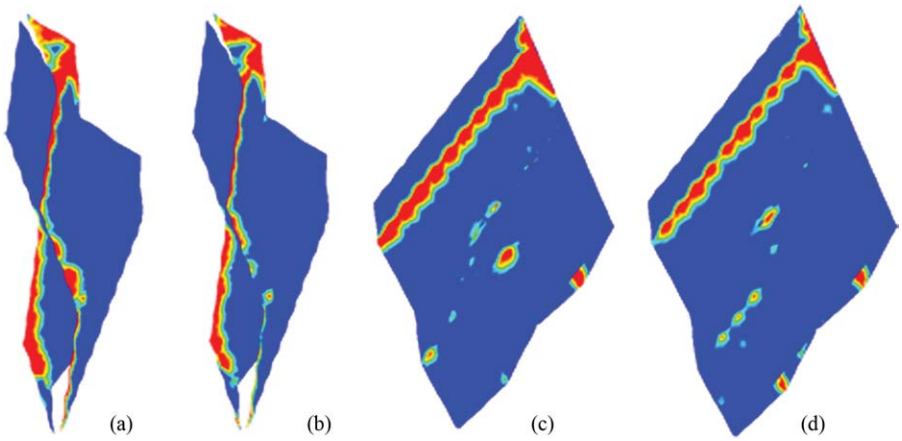


**Figure 6. Liquid film flow behavior on the structured packing.**

**(a) $L$=100 m$^3$/(m$^2$ h), (b) $L$=40 m$^3$/(m$^2$ h), (c) $L$=100 m$^3$/(m$^2$ h), (d) $L$=40 m$^3$/(m$^2$ h).**

than 0.03, which suggests that seldom liquid flows transverse to other units. It can also be observed that $L$ has little influence on $f$, $h$, $g$, and $hr$. Particularly for $hr$ and $h$, both of them are almost the same. For $f$ and $g$, because of the marginal change with $L$, they can also be considered as constants. The parameter $r$ declines with the increasing of $L$. Higher value of $r$ indicates a larger amount of liquid reflected to the internal of the column, and it is helpful to form a better distribution. Data of the stream split fraction coefficients are shown in Table 2. As the split fraction coefficients are dimensionless quantities, the parameter $r$ is correlated against Reynolds number, and it is defined as $Re=\rho_L u_L d/\mu_L$, where $u_L$ is the liquid velocity.

### *Liquid distribution in two pieces of packing sheets*

To validate the present model, a simulation of the same condition as that in Gu's work[36] is provided, in which the sole liquid flow distribution is measured in two pieces of Mellapak 350X packing sheets without holes or openings. The experimental equipment in Gu's work is illustrated in Figure 8. The height and width of the two pieces of packings are 200 mm and 400 mm, respectively. Water was fed into the packing surface from the distributor placed on the top of the two sheets, and it was collected by 10 reservoirs beneath the packing in order to measure the liquid distribution, each of which is 40 mm in width.

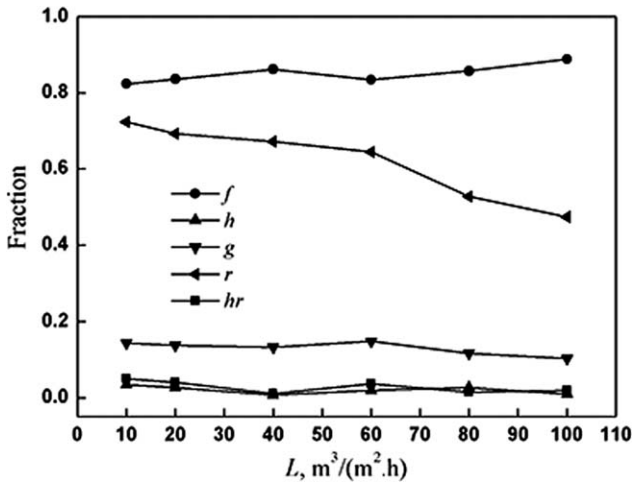


**Figure 7. The stream split fraction coefficients in different $L$.**

The liquid distribution simulation result of two pieces of structured packing obtained by the present and Gu's model is compared with the experimental data in Figure 9. In Figure 9a, it is well distributed in the condition of uniform feeding except a higher liquid distribution ratio at side wall of the column. A good agreement of experimental and simulation data is observed.

The liquid distribution result in the condition of single-point feeding is illustrated in Figure 9b. The liquid is fed in the middle of the packing at the top. It is found that the liquid scatters evidently as most of the liquid flows along the packing channel, and seldom flows vertical downward. It can also be observed that in the middle of the packing, both the models predict a higher value of liquid distribution ratio. The reason of that may be the underestimation of parameter $f$ which is caused by a smaller solid–liquid contact angle applied in the simulation. The comparison result shows that the CFD calculation of small scale can supply the parameters that the macro-scale calculation need. Moreover, the parameters in the present model reveal a degree of flexibility, and the stream split fraction can be varied according to the local liquid feed and no more a constant as in common mechanistic models. On the one hand, it makes the multi-scale simulation more precise, and on the other hand, it avoids any regression from experiment data at the expense of a certain amount of CFD computing. From the viewpoint of designing, no requisition for experiment data may be welcome albeit a moderate computing cost, which may not become a heavy burden for computers today.

### *Effective wetting area ratio*

The VOF simulation result can supply the interfacial information and the wetting ratio can be deduced. The effective wetting ratio $a_e/a_p$ predicted by the present model is offered in Figure 10 as well as the results by some other

**Table 2. Model Parameters**

| $f$ | $H$ | $hr$ | $r$ | $g$ |
|---|---|---|---|---|
| 0.85 | 0.020 | 0.028 | $\ln(2.14–1.5\times10^{-3}Re)$ ($R^2$=0.93) | 0.13 |

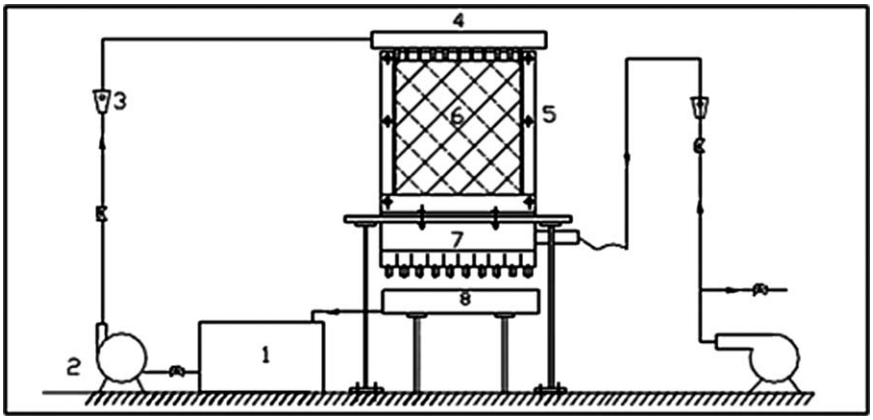


**Figure 8. The experimental equipment in Gu's work.**

**1. Water storage, 2. Centrifugal pump, 3. Rotameter, 4. Distributor, 5. Polymethyl methacrylate cover, 6. Packing sheet, 7. Water reservoir, 8. Recirculation groove.**

models in literatures. It can be found that the $a_e/a_p$ increases with the increase of $L$ in all cases. The value of $a_e/a_p$ predicted by Brito[37] and BRF[3,4] model is higher than 1 at some $L$. For Delft[5] model, the predicted values in different $L$ are all close to 1. The results of the present model and BS[38] model are somewhat similar and reasonable.

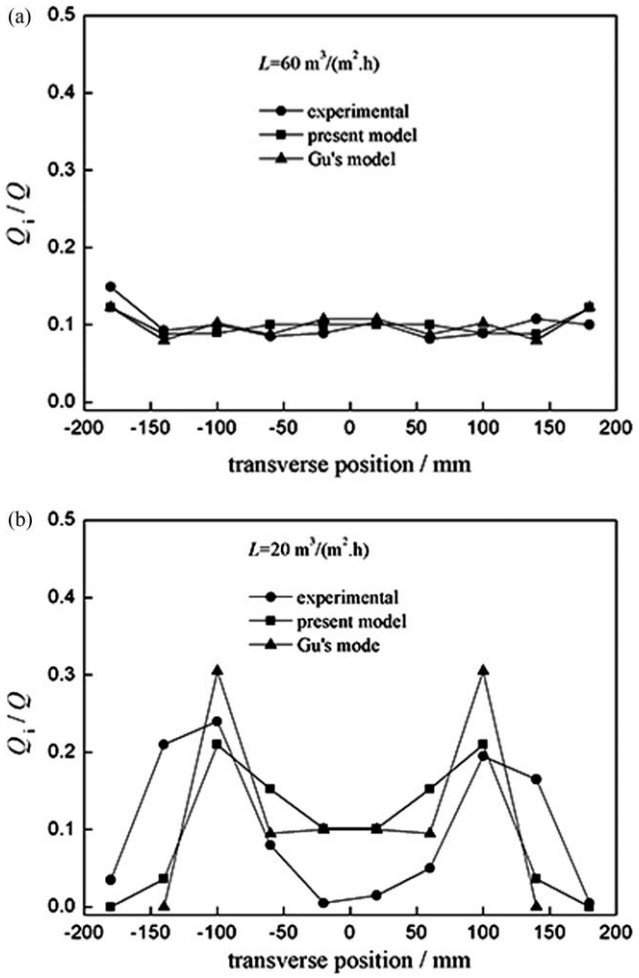


**Figure 9. The comparison of liquid distribution between unit network model and Gu's work.**

**(a) Uniform feeding, (b) Single-point feeding.**

The significant difference of the predicted $a_e/a_p$ is caused by different applicable conditions for the models mentioned, such as the packing type, operating condition, flow rate range of the liquid, and gas phase. The advantage of the present model is that the wetting ratio is deduced from VOF result and this approach has a high accuracy for any operating condition as long as the geometry can be precisely modeled.

### *Liquid holdup*

According to the result of effective wetting area ratio, the average liquid holdup is obtained by macro-scale calculation in the same condition of Gu's experiments and the result is illustrated in Figure 11. The averaged liquid holdup[39] is defined as

$$h_t = \frac{1}{N} \cdot \sum_{i=1}^{N} h_{ti} = \frac{1}{N} \cdot \sum_{i=1}^{N} \frac{a_{ei}}{a_{pi}} a_{pi} \delta_i \tag{12}$$

In Figure 11, it can be observed that the liquid holdup predicted by the present model agrees well with Gu's model and experimental results. Moreover, $h_t$ varies relatively significant under small $L$, which is well described by the present model. The good agreement of simulation and

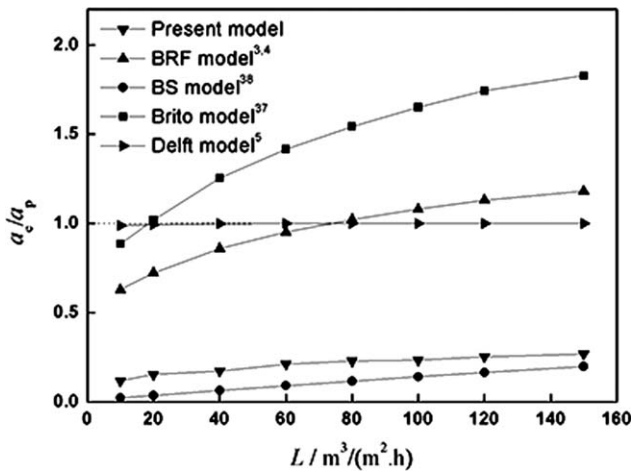


**Figure 10. Effective wetting area ratio predicted by different models.**

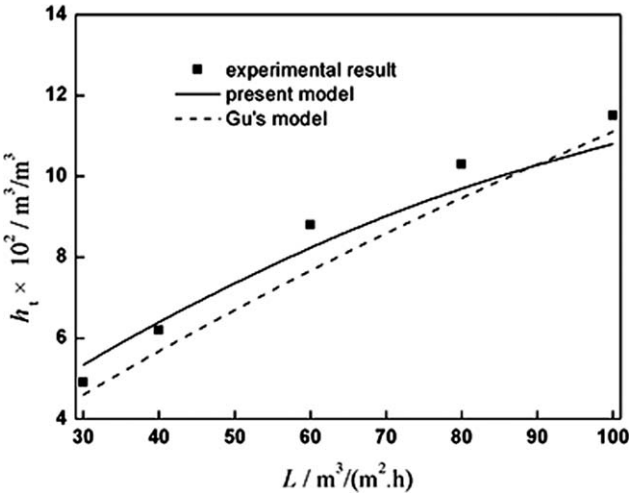


**Figure 11. The comparison of liquid holdup between unit network model and Gu's work.**

experimental results indicates a higher reliability of the effective wetting area ratio calculated by the present model, and it provides a power support for the subsequent study on the liquid distribution and holdup in packed column.

A 2-D liquid holdup distribution with uniform feeding in two pieces of structured packings is illustrated in Figure 12. The height and width of the packings studied are 200 mm and 400 mm, respectively. In Figure 12, it can be seen that $h_t$ close to the side wall is very small at the top, and then it increases when the liquid flows down. This phenomenon is called wall effect, which can be clearly depicted by the macro-scale calculation. As the side wall unit is not connected with each other, the $h_t$ in the interior unit between two side wall units is a little smaller, leading to a discontinuous increase of $h_t$ at sides. The $h_t$ in the middle, nearby the packing center, is a little higher because of more liquid flowing downward along the channel. In addition, the gradient of $h_t$ in Figure 12b decreases compared with the result in Figure 12a, and it indicates a better liquid distribution with the increased $L$.

Figure 13 gives the liquid holdup distribution with single-point feeding on the same packings mentioned in Figure 12. Because most of the liquid flows downward along the channels, the liquid holdup in the channels nearby is higher, and it decreases with the increase of the distance to the inlet. In addition, a higher $L$ leads to a larger $h_t$ in the cells, which indicates more liquid accumulates in the packing.

### *Liquid distribution in the structure packing column*

The liquid holdup distribution results of different layers of a column by 3-D macro-scale calculation are depicted in Figure 14. The column diameter is 0.4 m and the height of the packing layer is 0.2 m. The inlet is uniform feeding, and spray density is 80 m$^3$/(m$^2$ h). From Figure 14a, it can be found that, due to the anisotropy of structure packing, a single peak of liquid holdup can be found in the center, and the wall effect is also obvious. This is reasonable and compatible with the result in Figure 12. In Figure 14b, the liquid holdup distribution shows multi-peak structure and isotropy, which is a better distribution because most of the peaks are flat. The liquid holdup distribution results at the end of the fourth layer depicted in Figure 14d seems almost the same as that of the second layer except for the staggered direction. The above indicates how the preferential flow forms. The wall effects from 2nd to the 4th layer seem alike, and the region where the wall effect is serious is always changing. This is due to the reflection effect in side wall units.

To give a better understanding of the liquid distribution, Figures 15a–f give the liquid holdup distribution of different column layers with single-point feeding. At the end of the first layer shown in Figure 15a, liquid injected is limited between the two pieces of packing, and no liquid is observed at the side wall due to the limitation of the packing height. After the staggered arrangement of the second packing layer, liquid is extended and it transverses to form an area similar to rectangle, and the liquid holdup has four peaks at the four vertices of the rectangular region. After that, there are still some regions which are not wetted until the fourth layer shown in Figure 15d. At the end of the fourth layer, all the regions of the packing are covered with water and wall

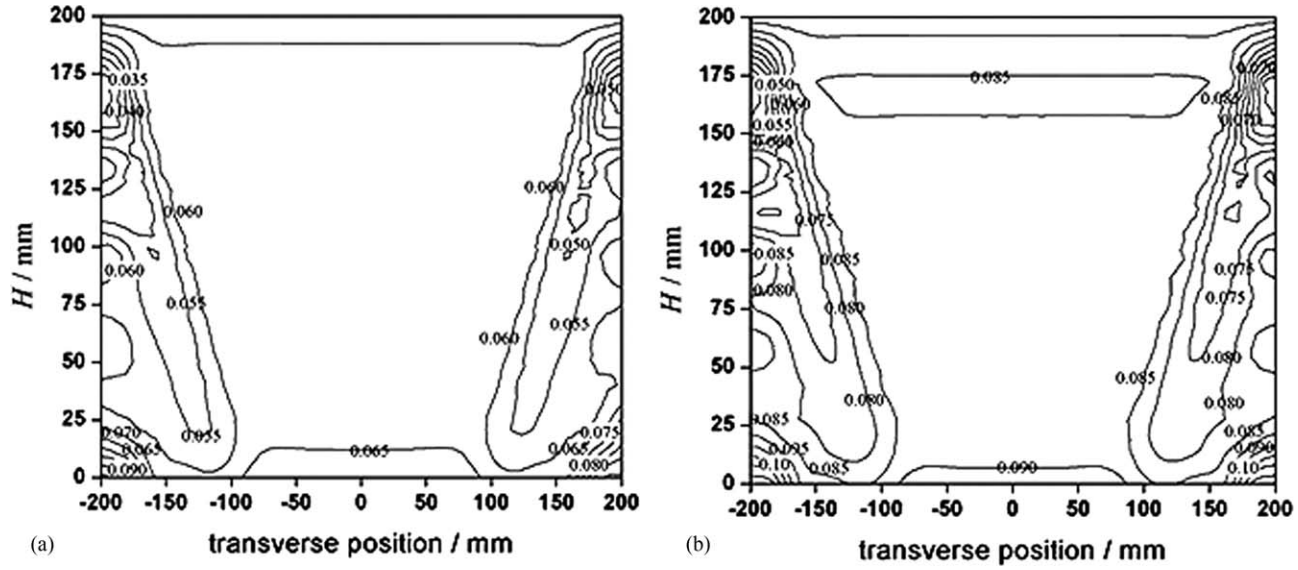


**Figure 12. Liquid holdup distribution in two pieces of packing with uniform feeding.**

**(a) $L$=40 m$^3$/(m$^2$ h), (b) $L$=60 m$^3$/(m$^2$ h).**

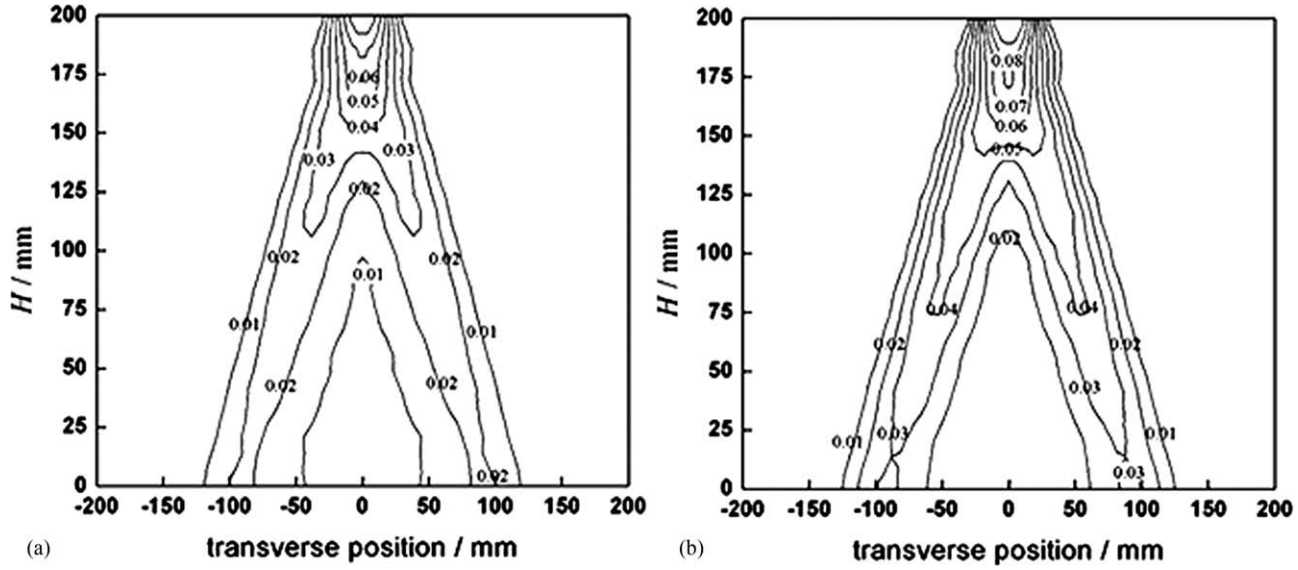


**Figure 13. Liquid holdup distributions in two pieces of packing with single-point feeding.**

**(a) $L$=40 m$^3$/(m$^2$ h), (b) $L$=60 m$^3$/(m$^2$ h).**

effect takes hold at the same time. With the increased number of packing layer, an even distribution is observed in Figure 15f.

## Discussion

The multi-scale calculation method proposed in this article aims to investigate the liquid distribution in the packed column. The small scale calculation is a VOF simulation inside the representative units, and the result can supply the stream split fractions and wetting area ratio to the macro-scale model. The macro-scale model is a mechanistic model, which considers all the possible stream splits in the packing cells. A validation of the multi-scale model is provided by the comparison of the calculation result of this model and the experiment liquid distribution data. Due to the lack of experiment liquid distribution data of gas–liquid counter-current, it is a pity that only a validation with merely liquid feed is performed. However, the present model has given good results, and the practicability and reliability of this method are proven in the article.

Although validation of the proposed model with merely liquid feed was given in the article, this model can certainly extend to other working conditions and other practical materials. Only the stream split fractions and wetting area ratio need to be changed, which are the communication between macro- and small-scale calculations, to get successful simulation of other structure packings such as 250Y, 500X, or other materials by adopting the appropriate properties. For some structured packings with holes or openings, the multi-scale model is also appropriate by adding another coefficient to describe the liquid flow through the holes or openings. The material used in this article is water–air system with the solid–liquid contact angle as 57°. The contact angle is determined by the properties of the material selected. It is commonly regarded that the solid–liquid contact angle affects the wetting of the packing surface greatly. In order to investigate the effect of the contact angle, we give an example of calculated liquid flow distribution in the condition of theoretical least contact angle, 0°. The result is shown in Figure 16. It can be apparently found that the packing surface still cannot be wetted completely, but the proportion of transverse flow is increased. The flow characteristic is significantly different with that in a larger contact angle as shown in Figure 6, and the stream split fraction coefficients in this condition are illustrated in

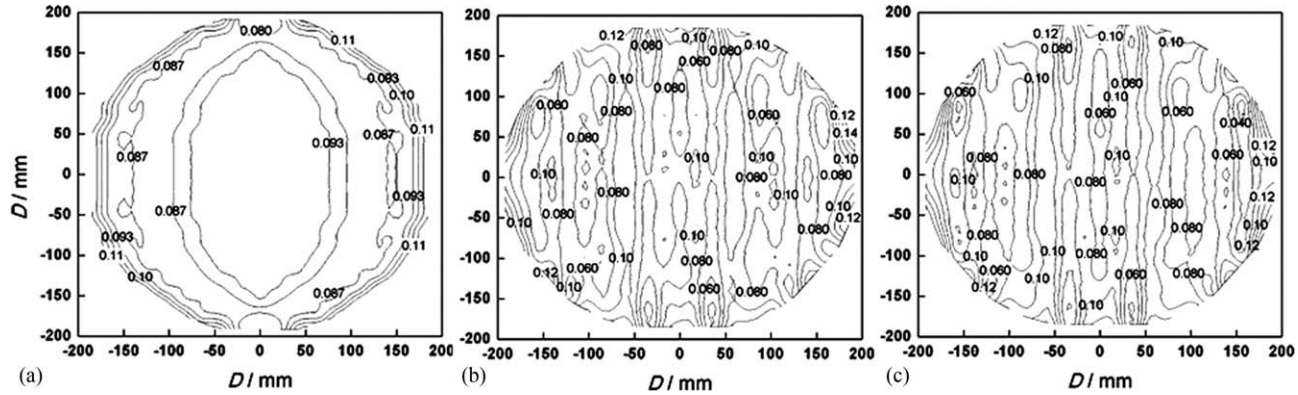


**Figure 14. Liquid holdup distributions in the column tray with uniform feeding.**

**(a) The first layer, (b) The second layer, (c) The fourth layer.**

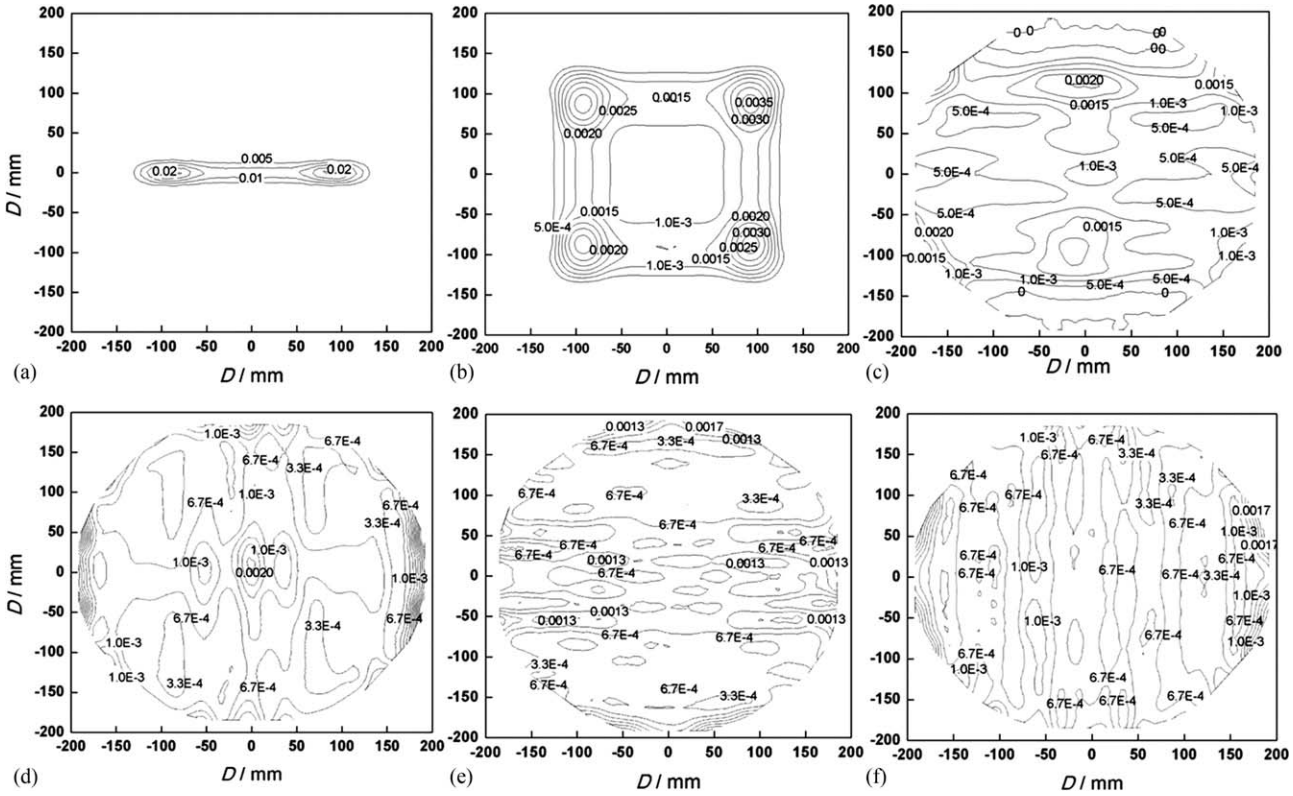


**Figure 15. Liquid holdup distributions in the column tray with single-point feeding.**

**(a) The first layer, (b) The second layer, (c) The third layer, (d) The fourth layer, (e) The fifth layer, (f) The sixth layer**

Table 3. The spray density range is 40 $m^3/(m^2\ h) \le L \le 100\ m^3/(m^2\ h)$.

Figure 17 shows the liquid flow behavior at the flow rate of 40 $m^3/(m^2\ h)$ with 0° contact angle and different $F$ factors. It is found that when $F = 1$, the liquid film is expanded and the wetting area increases due to the decreased liquid flow rate caused by the resistance of the gas phase and the increased proportion of transverse flow. When the $F$ factor increases to 2, the liquid film flowing transverse on the packing nearby is blown scattered to droplets, which incurs the small flow rate of transverse flow. While on the packing where the liquid flow rate is high, the liquid film is expanded by the impact of gas phase. And as higher gas velocity exists in the regions where liquid is blown scattered, it limits the increasing of the transverse flow ratio. The stream split fraction coefficients in these conditions are illustrated in Table 4.

## Conclusions

A new multi-scale model based on small-scale and macro-scale calculation is proposed in this article to provide an effective way to predict the liquid distribution in the structured packing column. The conclusions are as follows,

1. The small-scale calculation of the multi-scale model is VOF calculation inside the representative units, and the simulation is mostly precise by modeling the exact geometry of the structure packing cells. By summarizing the result of the VOF simulation to the stream split

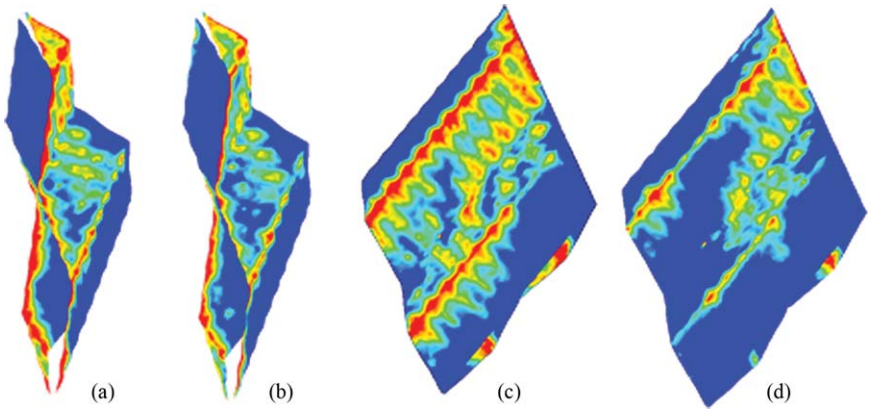


**Figure 16. Liquid film flow behavior with theoretical least contact angle.**

**(a) $L$=100 $m^3/(m^2\ h)$, (b) $L$= 40 $m^3/(m^2\ h)$, (c) $L$=100 $m^3/(m^2\ h)$, (d) $L$=40 $m^3/(m^2\ h)$.**

**Table 3. Model Parameters with Theoretical Least Contact Angle**

| $f$ | $h$ | $hr$ | $r$ |
|---|---|---|---|
| $0.08Re^{0.365}$ | $32Re^{-0.916}$ | $6.43Re^{-0.734}$ | $4.04 \times 10^{-6}Re^{2}-2.30 \times 10^{-3}Re + 0.607$ |
| ($R^2 = 0.86$) | ($R^2 = 0.93$) | ($R^2$=0.99) | ($R^2$=0.97) |

**Table 4. Model Parameters with 0° Contact Angle and Different $F$ Factors**

| $F$, (m/s)(kg/m$^3$)$^{0.5}$ | $f$ | $G$ | $h$ |
|---|---|---|---|
| 0 | 0.465 | 0.184 | 0.351 |
| 1 | 0.291 | 0.246 | 0.463 |
| 2 | 0.264 | 0.420 | 0.316 |

fraction coefficients, the macro-scale model, namely, the unit network model, can be conducted and the liquid distribution and the liquid holdup in the entire column can be predicted.

2. The results of small-scale calculation inside the representative units is summarized into the stream split fraction coefficients, *f, h, g, r, hr* in interior and side wall units, respectively. These parameters are theoretically variable with the local liquid feed of the representative units, which is different with other mechanistic models. In particular, for the air–water system with contact angle of 57° in the paper, *f*, *h*, *g* as well as *hr* can be considered as constants, but *r* decreases with increase of *L*. Furthermore, the parameters in the present model avoid any regression from experimental data, which is welcome for industrial design.
3. A good agreement of the liquid distribution and holdup predicted by the present model and the experimental data is obtained, which indicates a higher reliability of the model.
4. A heuristic extension of 3-D calculation of the entire column is further conducted to analyze the hydrodynamic characteristic in the entire column. A uniform feeding and single point feeding are applied, and the liquid holdup distributions are given.

With the present multi-scale model, the liquid holdup and distribution in the entire column have been successfully predicted. Moreover, the model can also be applied to simulate the gas–liquid two-phase hydrodynamic behavior for different experimental systems and packing geometries. The next step is to extend the application of the model to predict the concentration distribution in the entire column, which needs the proper assessment of mass-transfer coefficient in the representative units instead of the overall mass-transfer coefficient of the total column. The above mentioned suggests that the model of the article may support a more fundamental route to study the mass-transfer performance of the structure packing column. Based on the above consideration, this multi-scale method can be prospective for the analysis and design of distillation and absorption columns in chemical engineering.

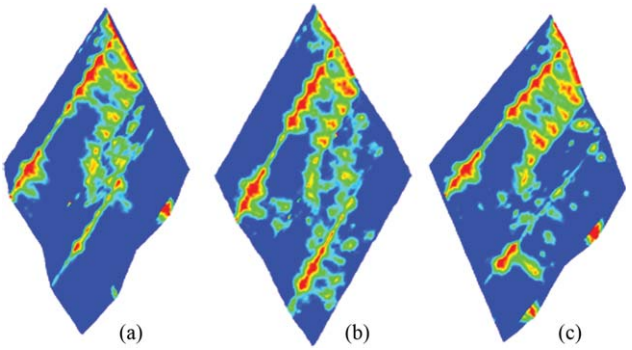


**Figure 17. Liquid film flow behavior in different *F* factors.**

**(a) $F = 0$, (b) $F = 1$ (m/s*(kg/m$^3$)$^{0.5}$), (c) $F = 2$ (m/s*(kg/m$^3$)$^{0.5}$).**


## Acknowledgments

The authors wish to acknowledge the financial support by the National Natural Science Foundation of China (project No. 21176171) and the National Program on Key Basic Research Project (project No. 2012CB720500).


## Notation

$a_e$ = wetting area, m$^2$/m$^3$
$a_p$ = specific area, m$^2$/m$^3$
$B$ = channel base, mm
$C$ = constant
$D$ = diameter of the packing tray, m
$d$ = hydrodynamic diameter, m
$F$ = source term of the momentum equation, N/m$^3$
$f$ = proportion of liquid flows along the channel
$f_i$ = interfacial friction factor
$G_k$ = the turbulence kinetic energy caused by averaged velocity gradient
$g$ = proportion of liquid mixing in the node
$H$ = packing height, m
$h$ = crimp height, mm
$h$ = proportion of liquid flows transverse in feature unit
$hr$ = proportion of liquid flows transverse in side wall unit
$h_t$ = liquid holdup, m$^3$/m$^3$
$k$ = turbulent kinetic energy, m$^2$/s$^2$
$L$ = spray density, m$^3$/m$^2$ h
$L$ = liquid flowing down along the left-inclining channel
$LWL$ = liquid flowing close to the left side wall
$LWR$ = liquid flowing close to the right side wall
$P_L = P_R$ = half of the liquid mixing in the node
$q$ = volume flow rate per unit of perimeter length, m$^3$/m s
$R$ = liquid flowing down along the right-inclining channel
$r$ = reflected part of the liquid flowing down along the side wall
$S$ = channel side, mm
$u$ = liquid velocity, m/s

### *Greek letters*

$\alpha$ = the reciprocal of effective Prandtl number
$\alpha$ = volume fraction
$a_e$ = effective interfacial area per unit volume, m$^2$/m$^3$
$\theta$ = corrugation angle of structured packing, °
$\rho$ = density, kg/m$^3$
$\sigma$ = surface tension, N/m
$\mu$ = dynamic viscosity, kg/s m or Pa s
$\varepsilon$ = porosity
$\kappa$ = free surface curvature, m$^{-1}$
$\varepsilon$ = turbulent dissipation rate, m$^2$/s$^3$
$\delta$ = thickness of the liquid film, m

### *Subscripts*

L = liquid phase
G = gas phase

## Literature Cited


1. Brunazzi E, Paglianti A. Mechanistic pressure drop model for columns containing structured packing. *AIChE J*. 1997;43:317–327.
2. Billet R, Schultes M. Prediction of mass columns with dumped and arranged packings: updated summary of the calculation method of Billet and Schultes. *Chem Eng Res Des*. 1999;77:498–504.
3. Rocha JA, Bravo JL, Fair JR. Distillation columns containing structured packings: a comprehensive model for their performance, Part 1: Hydraulic models. *Ind Eng Chem Res*. 1993;32:641–651.
4. Rocha JA, Bravo JL, Fair JR. Distillation columns containing structured packings: a comprehensive model for their performance, Part 2: mass transfer model. *Ind Eng Chem Res*. 1996;35:1660–1667.
5. Olujic Z, Kamerbeek AB, de Graauw J. A corrugation geometry based model for efficiency of structured distillation packing. Chem Eng Proc. 1999;38:683–695.
6. Hodson JS, Fletcher JR, Porter KE. Fluid mechanical studies of structured distillation packings. Institution of Chemical Engineers Symposium Series on Distillation & Absorption, *AIChE*, New York, 1997; 999–1007.
7. van Gulijk C. Using computational fluid dynamics to calculate transversal dispersion in a structured packed bed. *Comput Chem Eng*. 1998;22:767–770.
8. van Baten JM, Ellenberger J, Krishna R. Radial and axial dispersion of the liquid phase within a KATAPAK-S structure: experiments vs. CFD simulations. *Chem Eng Sci*. 2001;56:813–821.
9. van Baten JM, Krishna R. Liquid-phase mass transfer within KATAPAK-S structures studied using computational fluid dynamics simulations. *Catal Today*. 2001;69:371–377.
10. van Baten JM, Krishna R. Gas and liquid phase mass transfer within KATAPAK-S structures studied using CFD simulations. *Chem Eng Sci*. 2002;57:1531–1536.
11. Klöker M, Kenig EY, Gorak A. On the development of new column internals for reactive separations via integration of CFD and process simulation. *Catal Today*. 2003;79:479–485.
12. Klöker M, Kenig EY, Piechoia R, Burghoff S, Egorov Y. CFD-based study on hydrodynamics and mass transfer in fixed catalyst beds. *Chem Eng Technol*. 2005;28:31–36.
13. Egorov Y, Menter F, Klöker M, Kenig EY. On the combination of CFD and rate-based modelling in the simulation of reactive separation processes. *Chem Eng Proc*. 2005;44:631–644.
14. Petre CF, Larachi F, Iliuta I, Grandjean B. Pressure drop through structured packings: breakdown into the contributing mechanisms by CFD modeling. *Chem Eng Sci*. 2003;58:163–177.
15. Larachi F, Petre CF, Iliuta I, Grandjean B. Tailoring the pressure drop of structured packings through CFD simulations. *Chem Eng Proc*. 2003;42:535–541.
16. Raynal L, Boyer C, Ballaguet JP. Liquid holdup and pressure drop determination in structured packing with CFD simulations. *Can J Chem Eng*. 2004;82:871–879.
17. Khosravi Nikou MR, Ehsani MR, Turbulence models application on CFD simulation of hydrodynamics, heat and mass transfer in a structured packing. *Int Commun Heat Mass Transfer*. 2008;35:1211–1219.
18. Fernandes J, Simoes PC, Mota JPB, Saatdjian E. Application of CFD in the study of supercritical fluid extraction with structured packing: dry pressure drop calculations. *J Supercrit Fluids*. 2008;47:17–24.
19. Fernandes J, Lisboa PF, Simoes PC, Mota JPB Saatdjian E. Application of CFD in the study of supercritical fluid extraction with structured packing: wet pressure drop calculations. *J Supercrit Fluids*. 2009;50:61–68.
20. Szulczewska B, Zbicinski I, Gorak I. Liquid flow on structured packing: CFD simulation and experimental study. *Chem Eng Technol*. 2003;26:580–584.
21. Gu F, Liu CJ, Yuan XG, Yu GC. CFD. Simulation of liquid film flow on inclined plates. *Chem Eng Technol*. 2004;27:1099–1104.
22. Raynal L, Boyer C, Ballaguet JP. Liquid holdup and pressure drop determination in structured packing with CFD simulations. *Can J Chem Eng*. 2004;82:871–879.
23. Valluri P, Matar OK, Hewitt GF, Mendes MA. Thin film flow over structured packings at moderate Reynolds numbers. *Chem Eng Sci*. 2005;60:1965–1975.
24. Haroun Y, Raynal L, Legendre D. Mass transfer and liquid hold-up determination in structured packing by CFD. *Chem Eng Sci*. 2012;75:342–348.
25. Chen JB, Liu CJ, Yuan XG, Yu GC. CFD simulation of flow and mass transfer in structured packing distillation columns. *Chin J Chem Eng*. 2009;17:381–388.
26. Chen JB, Liu CJ, Li YK, Huang Y, Yuan XG, Yu GC. Experimental investigation of single-phase flow in structured packing by LDV. *Chin J Chem Eng*. 2007;15:821–827.
27. Mahr B, Mewes D. Two-phase flow in structured packings: modeling and calculation on a macroscopic scale. *AIChE J*. 2010;54:614–624.
28. Danziger R, Simulating the turbulent mixing process in a static mixing element. *Sulzer Tech Rev*. 1978;60:1–10.
29. Raynal L, Royon-Lebraud A. A multi-scale approach for CFD calculations of gas–liquid flow within large size column equipped with structured packing. *Chem Eng Sci*. 2007;62:7196–7204.
30. Jan BH, Seyed GE, André YT, Jules T. Parametric study for counter-current vapor-liquid free-surface flow in a narrow channel. *Cana J Chem Eng*. 2010;89:1–8.
31. Brackbill JU, Kothe DB, Zemach CA. Continuum method for modeling surface tension. *J Comp Phys*. 1992;100:335–354.
32. Woerlee GF, Berends J, Olujic Z, de Graauw J. A comprehensive model for the pressure drop in vertical pipes and packed columns. *Chem Eng J*. 2001;84:367–379.
33. Xu YY, Paschke S, Repke JU. Computational approach to characterize the mass transfer between the counter-current gas–liquid flow. *Chem Eng Technol*. 2009;32:1227–1235.
34. Stephan M, Mayinger F. Experimental and analytical study of countercurrent flow limitation in vertical gas/liquid flows. *Chem Eng Technol*. 1992;15:51–62.
35. Nusselt W. Die oberflaechenkondensation des Wasserdampfes. *Z Ver Dt Ing*. 1916;60:541–546.
36. Gu F, Liu CJ, Yuan XG, Yu GC. Liquid distribution model for sheet corrugated structure packing. *J Tianjin Univ*. 2005;38:586–591.
37. Brito MH, von Stockar U, Bangerter AM, Bomio P, Laso M. effective mass-transfer area in a pilot plant column equipped with structured packings and with ceramic rings. *Ind Eng Chem Res*. 1994;33:647–656.
38. Billet R, Schultes M. Fluid dynamics and mass transfer in the total capacity range of packed columns up the flood point. *Chem Eng Technol*. 1995;18:371–379.
39. Iliuta I. Mechanistic model for structured-packing columns: irrigated pressure drop, liquid holdup, and packing fractional wetted area. *Ind Eng Chem Res*. 2001;40:5140–5146.


*Manuscript received Dec. 25, 2012, and revision received Feb. 18, 2013.*